Therapeutics, Targets, and Chemical Biology

Cancer Research

Long-Chain Fatty Acid Analogues Suppress Breast Tumorigenesis and Progression

Udi Gluschnaider[1], Rachel Hertz[1], Sarit Ohayon[1], Elia Smeir[1], Martha Smets[1], Eli Pikarsky[2], and Jacob Bar-Tana[1]

Abstract

Obesity and type 2 diabetes (T2D) are associated with increased breast cancer incidence and mortality, whereas carbohydrate-restricted ketogenic diets ameliorate T2D and suppress breast cancer. These observations suggest an inherent efficacy of nonesterified long-chain fatty acids (LCFA) in suppressing T2D and breast tumorigenesis. In this study, we investigated novel antidiabetic MEDICA analogues consisting of methyl-substituted LCFA that are neither β-oxidized nor esterified to generate lipids, prompting interest in their potential efficacy as antitumor agents in the context of breast cancer. In the MMTV-PyMT oncomouse model of breast cancer, in which we confirmed that tumor growth could be suppressed by a carbohydrate-restricted ketogenic diet, MEDICA treatment suppressed tumor growth, and lung metastasis, promoting a differentiated phenotype while suppressing mesenchymal markers. In human breast cancer cells, MEDICA treatment attenuated signaling through the STAT3 and c-Src transduction pathways. Mechanistic investigations suggested that MEDICA suppressed c-Src–transforming activity by elevating reactive oxygen species production, resulting in c-Src oxidation and oligomerization. Our findings suggest that MEDICA analogues may offer therapeutic potential in breast cancer and overcome the poor compliance of patients to dietary carbohydrate restriction. *Cancer Res; 74(23); 6991–7002. ©2014 AACR.*

Introduction

Breast cancer is the most common invasive cancer in women. Mammary carcinoma develops in stages consisting of early hyperplastic ductal lesions that progress to adenoma, carcinoma *in situ* and lung metastasis. Mice expressing the Polyoma Middle T antigen (PyMT) driven by the mammary MMTV promoter (MMTV-PyMT) are widely used as the animal model for human breast cancer (reviewed in ref. 1). Thus, similarly to human tumors, mammary carcinoma in MMTV-PyMT mice develops in stages consisting of early hyperplastic lesions located on end buds of collecting ducts, which progress to adenoma/mammary intraepithelial neoplasia, carcinoma *in situ* and lung metastasis (2). PyMT-induced survival is due to a strictly ordered sequence whereby PyMT binds first to the protein phosphatase PP2A, followed by recruitment of a member of the c-Src family tyrosine kinases, usually $pp60^{c\text{-}src}$, to the PyMT/PP2A complex (3). Binding to PyMT/PP2A promotes c-Src "open" conformation and autophosphorylation of its Tyr416, resulting in activating its kinase activity and in phosphorylating PyMT tyrosines. Three of these phosphotyrosines act as binding sites for the SH2 or PTB domains of ShcA [PyMT (Tyr250)], PI3K [PyMT(Tyr315)], and PLCγ [PyMT(Tyr322)], resulting in activating the Ras/Raf/MEK/MAPK, PI3K/PDK1/Akt, and PLCγ/PKC survival pathways, respectively (1). Association of the PyMT/PP2A/c-Src complex with the plasma membrane is required for its transforming activity (4), implying that the complex may be visualized as an oncogenic receptor tyrosine kinase (RTK), with c-Src acting as its obligatory tyrosine kinase. In addition to c-Src, MMTV-PyMT breast cancer is driven by STAT3 (5), being activated by phosphorylation of its Tyr705 by activated c-Src (5–7) or JAK (8). Indeed, dephosphorylation of the gp130/JAK complex by the tyrosine phosphatase Shp2 is reported to result in suppressing PyMT-induced transformation, while knocking down Shp2 potentiates PyMT tumorigenesis (9). The c-Src/STAT3 interplay that drives PyMT-induced transformation is similar to that previously reported for the large tumor antigen of the Simian virus 40 (10, 11). Because 70% of human breast cancers express c-Src (12), whereas 50% express constitutive STAT3 (13), treatment strategies for suppressing the c-Src and STAT3 oncogenes of MMTV-PyMT breast cancer may be of relevance in treating human breast cancer (14).

Carbohydrate-restricted ketogenic diets, enriched in fat at the expense of carbohydrates, have been repeatedly reported to suppress breast cancer (15, 16). Tumor suppression by

[1]Department of Human Nutrition and Metabolism, Hebrew University Medical School, Jerusalem, Israel. [2]Department of Pathology, Hebrew University Medical School, Jerusalem, Israel.

Note: Supplementary data for this article are available at Cancer Research Online (http://cancerres.aacrjournals.org/).

U. Gluschnaider and R. Hertz contributed equally to this article.

Corresponding Author: Jacob Bar-Tana, Hebrew University Medical School, Ein-Kerem, Jerusalem, Israel 91120. Phone: 972-2-675-8305; Fax: 972-2-643-1105; E-mail: jacobb@ekmd.huji.ac.il

doi: 10.1158/0008-5472.CAN-14-0385

ketogenic diets has been ascribed to limiting insulin and IGF1 acting as growth factors (reviewed in ref. 17), and to the obligatory requirement of malignant cells for glucose-derived metabolites (e.g., nucleotides, NADPH) for supplying their biomass demands (Warburg effect, reviewed in ref. 18). Indeed, breast cancer is promoted by insulin resistance/hyperinsulinemia, and insulin sensitizers used for treating type 2 diabetes (e.g., metformin) appear to be effective in suppressing tumorigenesis in general and breast cancer in particular (19). Alternatively, the efficacy of ketogenic diets in suppressing tumorigenesis may further be ascribed to the inherent efficacy of free/nonesterified long-chain fatty acids (LCFA), if allowed to reach high enough intracellular concentrations. Carbohydrate restriction may indeed allow for that, by limiting the availability of glycerol-3-phosphate and insulin required for the esterification of LCFA into downstream lipid products (20).

The putative inherent efficacy of nonesterified LCFA to suppress transformation may be simulated by MEDICA analogues. MEDICA analogues (21) consist of long-chain, α,ω–dioic acids [HOOC–C(α′)–C(β′)–*Q*–C(β)–C(α)–COOH, where *Q* represents a long-chain core element], substituted in the αα′ (Mαα), ββ′ (Mββ), and/or other optional core carbons. MEDICA analogues may be thioesterified to their respective CoA-thioesters, but these are not esterified into lipids, nor converted into ceramides, whereas the substitutions at the αα′ or ββ′ positions block their β-oxidation. MEDICA analogues are mostly excreted in bile as respective glucuronides. As such, MEDICA analogues may mimic allosteric activities of free/nonesterified LCFA, while avoiding their role as substrates for β-oxidation or esterification into lipids. Moreover, MEDICA analogues proved antidiabetic hypolipidemic efficacy in a series of obese diabetic animal models (22–24, 26), prompting our interest in studying the efficacy of ketogenic diet and MEDICA in the breast cancer context.

Materials and Methods

Animals and diets

FVB wild-type females (Harlan Inc.) were bred in-house with FVB MMTV-PyMT heterozygous males (Dr. Itay Ben-Porat, Hebrew University Medical School, Jerusalem, Israel). F1-generation females were genotyped by PCR using the PyMT primers: Fw: 5′GGAAAGTCACTAGGAGC-AGGG 3′; Rev: 5′ GGAAGCAAGTACTTCACAAGGG 3′. Mice were kept in standard SPF conditions in 12 hours light/dark periods, with free access to food and water. Mice were fed with Teklad 2018S standard rodent diet (54% carbohydrate, 18% fat, and 24% protein energy), or with Teklad 93075 high-fat diet (HFD; 24% carbohydrate, 54.8% fat, and 21.2% protein energy), or with Teklad 96355 ketogenic diet (0.4% carbohydrate, 90.5% fat, and 9.1% protein energy). Teklad 96355 diet was freshly prepared as gelatin chips every 3 days. The MEDICA diet consisted of 0.04% (w/w) MEDICA [$HOOC–C(CH3)_2–(CH_2)_{12}–C(CH3)_2–COOH$] mixed in Teklad 2018S standard rodent diet (yielding a dose of 40 mg MEDICA/kg body weight/day). Energy intake was determined by measuring food consumption every 3 days. Two hours before sacrifice, mice were injected with bromodeoxyuridine (BrdUrd) i.p where indicated. Upon sacrifice, mice were anesthetized using 85% ketamine/15% xylazine (0.1 ml per 25–30 g body weight). Breast tumors and lungs were sampled in buffered 4% formaldehyde for further histochemistry/immunohistochemistry analysis, or in liquid nitrogen for RNA and protein analysis. Animal care and experimental procedures were in accordance with the accredited animal ethics committee of the Hebrew University Medical School.

Immunohistochemistry

Mammary tumor specimens fixed in 4% buffered formaldehyde were embedded in paraffin. Sections (5 μm) were dewaxed and rehydrated through graded ethanol dilutions, followed by cooking in 25 mmol/L citrate buffer, pH 7.4, at 115°C for 3 minutes. Endogenous peroxidase activity was blocked with 3% hydrogen peroxide. Sections were then incubated with the primary antibodies as indicated, followed by incubation with horseradish peroxidase (HRP) or fluorescent-conjugated secondary antibodies (The Jackson Laboratory). HRP-incubated sections were counterstained with hematoxylin. Fluorescent intensity was analyzed by confocal microscopy using DAPI for nuclei visualization (Zeiss LSM 710; Axio observer Z1). Lungs were excised and fixed in formalin overnight and then paraffin-embedded. Sections (5 μm) were stained with hematoxylin and eosin (H&E) and analyzed using computerized microscopy (Ariol SL-50; Olympus BX61 Applied Imaging).

Cell cultures

MMTV-PyMT primary cells were isolated from 16-week-old MMTV-PyMT mice as described previously (25). Met-1 cells (Dr. Alexander Borowsky, Center for Comparative Medicine, University of California, Davis, Davis, CA) and primary cells were cultured in complete DMEM (Biological Industries) supplemented with penicillin–streptomycin solution, L-glutamine, and 10% FCS, followed by adding MEDICA as indicated. Cell proliferation was quantified using the Methylene Blue assay. Met-1 cells cultured in 24 plate were transfected with M67-TATA-TK-LUC (1 μg) reporter plasmid, expression plasmids for constitutive STAT3 (0.1 μg), and for CMV–β-galactosidase (0.1 μg), using jetPEI DNA transfection reagent (26). Following 8 hours, medium was changed and cells were treated for 24 hours with MEDICA as indicated. Luciferase activity normalized to β-galactosidase was measured as previously described (26). HCC1954 cells (ATCC CRL-2338) were cultured in RPMI-1640 (Biological Industries) supplemented with penicillin–streptomycin solution and 10% FCS, and added MEDICA as indicated. Where indicated, HCC1954 cells were infected with lentivirus knockout constructs of sh-c-Src, sh-STAT3, or scramble plasmids (Sigma Mission), followed by puromycin selection.

Clonogenic assay

Cells of respective experimental plates were trypsinized. A total of 7,500 cells were plated on 60-mm plate and allowed to form colonies for 10 days. Cells were fixed with 0.625% gluteraldehyde and stained with methylene blue. Colonies exceeding 400 μm in size were counted.

Cell lysis and Western blotting

Cultured cells were scraped with 1X lysis buffer (50 mmol/L Tris HCl pH 8.0, 1% Triton X-100, 1 mmol/L EGTA, 1 mmol/L EDTA, 150 mmol/L NaCl, 5 mmol/L NaPPi, 50 mmol/L NaF, 1 mmol/L PMSF, 1 mmol/L Na Vanadate, 40 nmol/L bpVfan and protease inhibitor cocktail (Sigma), and centrifuged for 15 minutes at 12,500 rpm. Frozen tumor samples were homogenized in lysis buffer using Polytron homogenizer. Protein concentration was determined by BCA (Thermo Scientific). Unless otherwise indicated, protein lysates were prepared in SDS sample buffer [62 mmol/L Tris (pH 6.8), 2.3% SDS, 0.64 mmol/L mercaptoethanol, 10% glycerol], subjected to SDS-PAGE, electrotransferred onto cellulose nitrate membranes (Schleicher & Schuell) and probed with the indicated first antibody, followed by HRP-labeled second antibody. Where indicated, protein lysates were prepared in SDS sample buffer lacking mercaptoethanol. Bands were detected by ECL, and the intensity of individual bands was determined by densitometry using TINA 2.10 software.

Immunoprecipitation

MET-1 cells were incubated as indicated. Following incubation, cells were rinsed once in cold PBS and lysed with 50 mmol/L Hepes (pH 7.4), 150 mmol/L NaCl, 10% glycerol, 1.5 mmol/L MgCl2, 1 mmol/L EGTA, 1% Triton, 50 mmol/L β-glycerolphosphate, 25 mmol/L NaF, 1 mmol/L Na-vanadate, 40 nmol/L bpVphen, protease inhibitor mix (Sigma), and 17.5 mg/mL Octyl beta-D-glucopyranoside (Sigma). Lysates were kept on ice for 30 minutes and centrifuged at 12,000 rpm for 15 minutes. Lysate of 250 μg was incubated for 4 hours with protein A/G beads (Santa Cruz Biotechnology) preloaded with the indicated antibody . The immunoprecipitate was rinsed three times with washing buffer [20 mmol/L Hepes (pH 7.4), 150 mmol/L NaCl, 0.1%Tx-100, 10% glycerol], suspended in SDS sample buffer and boiled for 8 minutes. Immunoprecipitated proteins were analyzed by SDS-PAGE/Western blotting.

qRT-PCR

RNA was purified from frozen mouse tissues using the Total RNA Mini Kit (Geneaid). RNA of 0.5 μg was used as template for cDNA synthesis using M-MLV reverse transcriptase (Invitrogen) . Real-time PCR was carried out (Rotorgene, Corbett Research) using KAPA SYBR FAST qPCR MIX (Kapa Biosystems) with the following primers (5′ to 3′): MMP9 (Fw: AACCTCCAACCTCACGGACAC, Rev: CTGCT-TCTCTC-CCATCATCTGG); E-cadherin (Fw: TCATCATTGAGAGGGA-GACAGGCT, Rev: TGGGTAAACTCTGGCCTGTTGTCA); Ezh2 (Fw: GACGATGATGGAGATGA-TCCAGATG, Rev: CCGAG-GTGGGCAAGTTTCTTTATC); PyMT (Fw: CTCCAACAGAT-CACCCGCACATACT, Rev: GCTGGTCTTGGTCGCTTTCTG-GA-TAC). mRNA was quantified using the $\Delta\Delta C_t$ method (27).

ELISA

VEGF content of mouse lysates was determined using the Quantikine Mouse VEGF Kit (R&D System) according to the manufacturer's instructions.

ROS production

Reactive oxygen species (ROS) production was determined by 2,7 dichlorofluoresceine diacetate (DCF; 5 μmol/L) added to respective cell cultures for the last 15 minutes of incubation. Cells were washed once with PBS, and lysed with 0.5% TX-100. DCF fluorescence was determined by 485/530 nm excitation/emission analysis. Hydrogen peroxide production was determined by incubating respective growth media (phenol red-free) with HRP/Amplex Red (Invitrogen). Fluorescence was determined by 560/590-nm excitation/emission analysis. The glutathione/glutathione disulfide (GSH/GSSG) ratio was determined by the GSH/GSSG-Glo assay (Promega) according to the manufacturer's protocol.

Antibodies

Anti–β-casein, anti-Erk, and anti–phospho-Erk(Tyr204) antibodies were from Santa Cruz Biotechnology; anti-pHH3, anti-Akt, anti–phospho-Akt(Ser473), anti–phospho-c-Src(Tyr416), anti–phospho-c-Src(Tyr527), anti–cleaved caspase-3, anti–phospho-FAK(Tyr925), anti–phospho-p130CAS(Tyr910) antibodies were from Cell Signaling Technology; anti–c-Src and anti-Ezh2 antibodies were from Millipore; anti-BrdUrd antibody was from Thermo Scientific; anti-CD34 antibody was from Cedarlane; anti–E-cadherin, anti–β-catenin, anti-p130CAS, and anti-FAK antibodies were from BD Transduction Laboratories; antitubulin antibody was from Sigma. c-Src kinase inhibitors were from LC Laboratories.

Statistical analysis

Statistical analysis was performed by two-tailed homoscedastic repeated measure ANOVA. Significance was analyzed by the paired *t* test.

Results

Suppression of MMTV-PyMT tumor growth by carbohydrate restriction

Suppression of MMTV-PyMT tumorigenesis by ketogenic diet has been verified in transgenic FVB MMTV-PyMT mice fed throughout weeks 4 to 12 with either standard, high-fat or ketogenic diet, consisting of 3.2, 0.4, and 0.004 carbohydrate/fat energy ratios, respectively. Tumor mass decreased by 65% upon increasing dietary fat energy at the expense of dietary carbohydrate (Fig. 1A), with increase in tumor latency (not shown). Suppression of tumor mass by ketogenic diet was accompanied by decrease in BrdUrd staining (Fig. 1B). The extent of decrease in tumor mass by ketogenic diet was essentially similar to that of MEDICA dosed with standard carbohydrate-rich diet (Fig. 1A).

Suppression of MMTV-PyMT tumorigenesis by ketogenic diet was not accounted for by caloric restriction that may accompany use of ketogenic diets (15). Indeed, daily energy consumption amounted to 9.3, 10.2, 16.0, and 14.1 kcal/mouse for the standard, high-fat, ketogenic diet, and MEDICA feed, respectively. The 150% to 170% increase in ketogenic energy consumption did not result in any significant change in body weight gain (23.4 ± 2.3, 22.5 ± 1.3, and 23.5 ± 2.4 g for 12 weeks control, ketogenic and MEDICA mice, respectively). In the absence of visible diarrhea or steatorrhea, the increase in

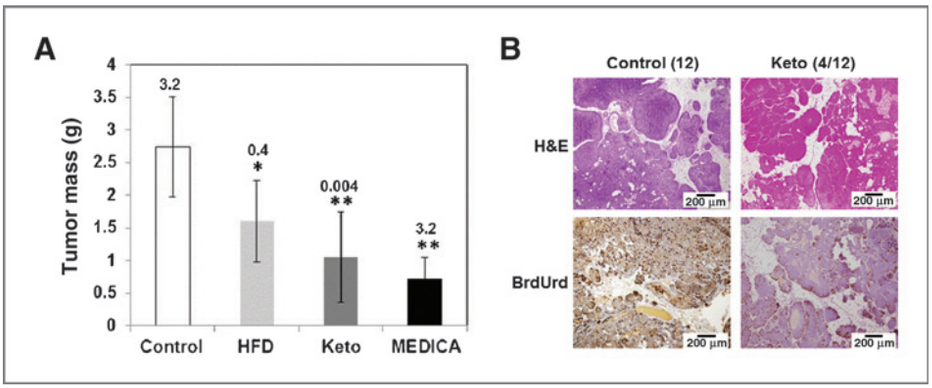

Figure 1. Suppression of MMTV-PyMT tumorigenesis by ketogenic diet. A, MMTV-PyMT female mice were fed *ad libitum* from weaning (4 weeks of age) to 12 weeks with standard rodent diet (Control), HFD (Teklad 93075), ketogenic diet (Keto; Teklad 96355), or standard rodent diet mixed with MEDICA. Upon sacrifice, breast tumors were dissected and weighed to yield total body tumor mass. Numbers, respective dietary carbohydrates/fat energy ratio. Mean ± SE (n = 8–10 mice/group); *, significant as compared with control diet ($P < 0.05$); **, significant as compared with control diet ($P < 0.002$). B, representative photomicrographs (×20) of MMTV-PyMT breast tumors of mice maintained on standard (Control) or ketogenic (Keto) diet throughout weeks 4 to 12. Sections were stained with H&E and immunostained with BrdUrd as described in Materials and Methods.

energy consumption may imply an increase in total body energy turnover of MMTV-PyMT mice maintained on ketogenic diet or MEDICA feed.

Suppression of MMTV-PyMT tumorigenesis by MEDICA

MEDICA treatment of transgenic FVB MMTV-PyMT female mice throughout weeks 4 to 12 or weeks 4 to 18 (denoted by 4/12 and 4/18, respectively) resulted in 75% decrease in tumor mass as compared with control mice (Fig. 2A). Suppression of tumor growth was also reflected in longer tumor latency in MEDICA-treated mice, in which palpable tumors of MEDICA-treated mice were delayed by 2 weeks as compared with control mice (10 and 8 weeks, respectively). Moreover, MEDICA treatment throughout weeks 12 to 18 (denoted by 12/18) resulted in robust decrease in tumor mass (Fig. 2A), implying growth suppression of established MMTV-PyMT tumors.

Nontreated tumors consisted of highly dense poorly differentiated mammary carcinoma, whereas MEDICA-treated tumors consisted of areas of papillary glandular structures, with occasional cysts lined by squamous epithelium and filled with fluid containing casein (Figs. 2B and C), implying more differentiated morphologic pattern.

Most importantly, MEDICA treatment resulted in robust decrease in lung metastases (Fig. 2D). Thus, the number of lung metastatic foci, and in particular the percentage of lung area occupied by lung metastases, were significantly decreased by MEDICA (12/18) treatment (5.9% vs. 0.4% lung area in nontreated and MEDICA-treated mice, respectively), implying growth inhibition of established lung metastatic foci.

Suppression of MMTV-PyMT tumor growth by MEDICA was not accounted for by loss of the PyMT transgene, or by interfering with the overall hormonal balance of treated mice. Thus, PyMT expression remained unaffected by MEDICA treatment, and MEDICA-treated female mice were fertile (not shown).

Suppression of MMTV-PyMT tumor growth by MEDICA was further evaluated in terms of proliferation, apoptosis, and angiogenesis. MEDICA treatment resulted in pronounced decrease in BrdUrd incorporation, being sparse and mainly evident at the periphery of tumor lesions (Fig. 3A). In line with decreased BrdUrd incorporation, MEDICA treatment resulted in 75% decrease in the tumor mitotic index verified by p-HH3 staining (Fig. 3B). Inhibition of proliferation by MEDICA was accompanied by increase in apoptosis, verified by cleaved caspase-3 staining (Fig. 3C). Increased apoptosis was mainly evident in tumor samples of MEDICA (4/18), whereas decreased proliferation was mostly pronounced in tumor samples of MEDICA (4/12). Suppression of MMTV-PyMT tumor growth by MEDICA was further accompanied by decrease in tumor vascularization as verified by decrease in the CD34 endothelial marker (Fig. 3D) and tumor VEGF content (Fig. 3E).

MMTV-PyMT mesenchymal–epithelial transition in response to MEDICA

The higher epithelial differentiation pattern induced by MEDICA, combined with inhibition of MMTV-PyMT metastasis, was further evaluated by verifying epithelial–mesenchymal biomarkers in response to MEDICA (Fig. 4). MEDICA treatment resulted in increase in E-cadherin expression (Fig. 4A), being accompanied by increase in membranous β-catenin (Fig. 4B), with pronounced decrease in MMP9 expression (Fig. 4C). MEDICA-induced expression of E-cadherin combined with suppression of MMP9 expression was further evaluated in terms of transcription factors that may control mesenchymal–epithelial transition (MET). Ezh2 (polycomb group protein enhancer of zeste homolog 2) is the histone methyltransferase catalytic subunit of the polycomb-repressive complex 2, being overexpressed in a variety of aggressive breast cancers (28, 29). Ezh2 is associated with genome instability, disruption of mammary ductal morphogenesis (30), and invasion and metastasis of malignant breast cancer, being partly accounted for by suppression of E-cadherin and induction of MMPs expression (31, 32). Ezh2 transcript, protein, and cell content

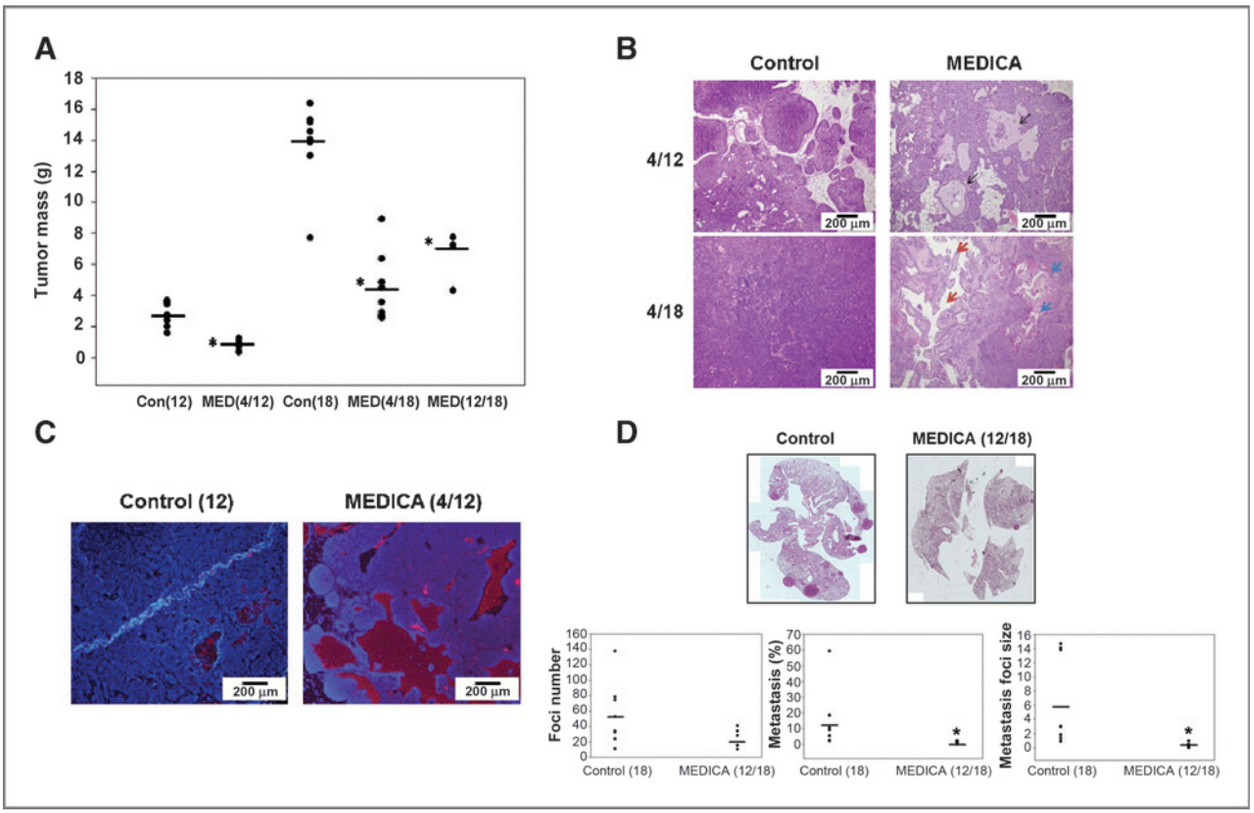

Figure 2. Suppression of MMTV-PyMT tumorigenesis by MEDICA. MMTV-PyMT female mice were fed *ad libitum* for 12 weeks (control, $n = 8$; ref. 12) or 18 weeks (control, $n = 9$; ref. 18) with standard rodent diet (Teklad 2018) in the absence or presence of added MEDICA (0.04% w/w), from weeks 4 to 12 [MEDICA (4/12)] ($n = 8$), weeks 4 to 18 [MEDICA (4/18)] ($n = 8$), or weeks 12 to 18 [MEDICA (12/18)] ($n = 5$) as indicated. A, upon sacrifice, breast tumors were dissected and weighed to yield total tumor mass. Points, total tumor mass of individual mice; lines, mean value of each group; *, significant as compared with respective control ($P < 0.001$). B, representative H&E-stained photomicrographs of MMTV-PyMT tumors of control, MEDICA (4/12), and (4/18)–treated MMTV-PyMT mice. Note the cystic (black arrows), papillary (red arrows), and squamous-like (blue arrows) structures. C, representative β-casein–immunostained photomicrographs of control and MEDICA (4/12) tumors. D, representative H&E-stained lung photomicrographs of control and MEDICA (12/18)-treated MMTV-PyMT mice. Metastasis appears as dark spots. Number of metastatic foci and the percentage fraction of metastatic area per lung were determined by computerized quantitative histology of respective H&E-stained lung photomicrographs. Points, values of individual mice; lines, median value of each group; *, significant as compared with control ($P < 0.05$).

were suppressed by MEDICA (Fig. 4D), pointing to mammary epithelial transition of MEDICA-treated MMTV-PyMT tumors.

Suppression of PyMT c-Src and STAT3 oncogenic drivers by MEDICA

Suppression of the MMTV-PyMT oncogenic drivers by MEDICA was evaluated in Met-1 (33) and primary MMTV-PyMT cells. MEDICA inhibited the proliferation of primary MMTV-PyMT and of Met-1 cells (Fig. 5A). The μmol/L concentrations of MEDICA reflect the high binding affinity of MEDICA analogues to serum albumin [higher than 99%, independently of MEDICA concentrations in the range of 0–0.9 mmol/L (not shown)], resulting in nmol/L concentrations of the free MEDICA acid in the culture medium.

The roles played by the c-Src and STAT3 transduction pathways in PyMT cell survival were verified in Met-1 cells. In line with the transforming role played by c-Src/PyMT, cell growth was inhibited by the c-Src kinase inhibitor dasatinib (Supplementary Fig. S1A; ref. 34). However, cell growth was only partially suppressed by dasatinib under saturating dasatinib concentrations, whereby phospho–c-Src(Tyr416) was 90% inhibited, implying the activity of additional oncogenic driver(s). Indeed, Met-1 cell growth was inhibited by the JAK/STAT3(Tyr705) inhibitor pyridine 6 (P6) (Supplementary Fig. S1B; ref. 13), indicating that STAT3 serves as oncogenic driver for PyMT cell survival. However, here again suppression of Met-1 cell growth by P6 was only partial, whereby phospho-STAT3(Tyr705) was essentially abrogated, implying that Met-1 survival is driven by each of the c-Src and STAT3 oncogenes. Moreover, phospho-STAT3(Tyr705) of Met-1 cells was only marginally (<20%) inhibited by the c-Src inhibitor dasatinib (not shown), whereas phospho–c-Src(Tyr416) was not affected by the JAK inhibitor P6, indicating that the c-Src and STAT3 transduction pathways act as independent oncogenic drivers. In line with that, inhibition of Met-1 cell growth by combining dasatinib and P6 was additive (Supplementary Fig. S1C), implying that Met-1 survival is independently driven by both, c-Src and STAT3.

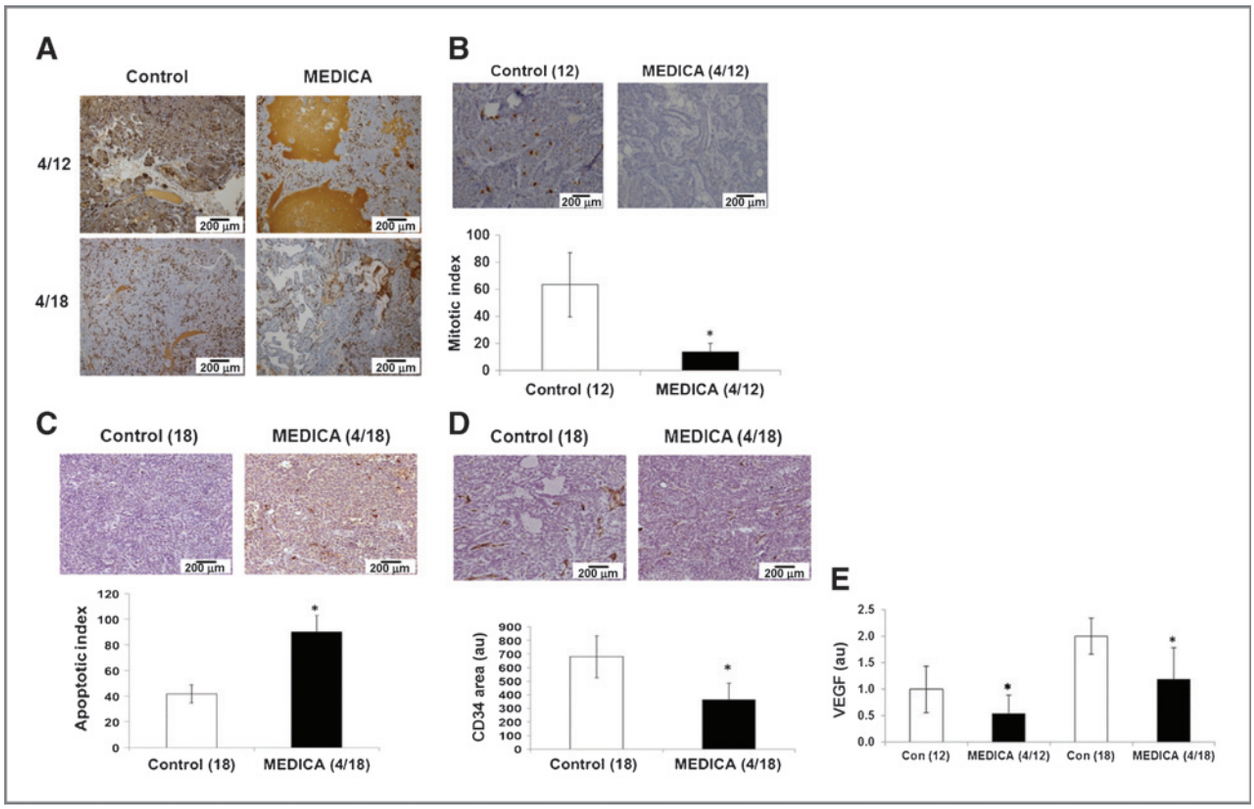

Figure 3. MMTV-PyMT tumor proliferation, apoptosis, and angiogenesis in response to MEDICA. MMTV-PyMT female mice were fed *ad libitum* with standard rodent diet (Telkad 2018) in the absence or presence of added MEDICA (0.04% w/w) from weeks 4 to 12 (4/12) or weeks 4 to 18 (4/18) as indicated. A, representative BrdUrd-immunostained photomicrographs of MMTV-PyMT tumors of control, MEDICA (4/12)-, and (4/18)-treated mice. Cysts are stained in brown. B, representative P-HH3–immunostained photomicrographs of MMTV-PyMT tumors of control and MEDICA (4/12)-treated mice. The mitotic index was determined by counting the number of p-HH3–stained cells of 10 fields per mouse. Mean ± SE ($n = 8$); *, significant as compared with control ($P < 0.05$). C, representative photomicrographs of cleaved caspase-3 immunostaining of MMTV-PyMT tumors of control and MEDICA (4/18)-treated mice. The apoptotic index was determined by counting the number of cleaved caspase-3–stained cells of 10 fields per mouse. Mean ± SE ($n = 6$); *, significant as compared with control ($P < 0.05$). D, representative CD34-immunostained photomicrographs of MMTV-PyMT tumors of control and MEDICA (4/18)-treated mice. Total CD34-stained area was determined by screening the CD34-stained area of 10 fields per mouse using computerized microscopy; *, significant as compared with control ($P < 0.05$). E, VEGF content of MMTV-PyMT tumors of control and MEDICA-treated mice. VEGF content was determined by ELISA in tumor lysates of control, MEDICA (4/12)-, and MEDICA (4/18)-treated mice. VEGF content of 12-week control is defined as 1.0 mean ± SE ($n = 8$); *, significant as compared with the respective control ($P < 0.001$).

In line with our previous findings in other cell types (26), MEDICA treatment resulted in suppressing STAT3(Tyr705) and Akt(Ser473) phosphorylation in primary MMTV-PyMT cells, and in suppressing the transcriptional activity of STAT3 in Met-1 cells (Fig. 5B), indicating that suppression of PyMT survival by MEDICA may partly be ascribed to inhibition of the STAT3 transduction pathway. MEDICA efficacy in suppressing c-Src/PyMT was pursued by analyzing the c-Src content in PyMT immunoprecipitates of Met-1 cells. MEDICA treatment resulted in abrogating c-Src association with PyMT (Fig. 5C), implying suppression of c-Src–induced PyMT transduction. MEDICA apparent efficacy in inducing a conformational change in c-Src was further indicated by probing c-Src sensitivity to dasatinib in the absence and presence of added MEDICA. Indeed, dasatinib concentrations that were only partly effective in inhibiting phspho-Src(Tyr416), became fully effective by added MEDICA, implying an apparent MEDICA-induced increase in c-Src affinity for dasatinib (Fig. 5D). MEDICA-induced increase in c-Src affinity for dasatinib was further verified by the combined effect of MEDICA and dasatinib in suppressing Met-1 cell growth, under conditions of short incubation time (24 hours), whereby MEDICA stand-alone was essentially ineffective in suppressing cell growth. Added MEDICA resulted in synergizing dasatinib activity in suppressing Met-1 cell growth by dasatinib concentrations that were only partially effective in the absence of MEDICA (Fig. 5E). That is in contrast with P6, in which its combination with dasatinib was strictly additive (Supplementary Fig. S1C). The mode of action of MEDICA in suppressing c-Src–transforming activity has been further studied in human HCC1954 breast cancer cells (overexpressing ErbB2, ER-, and PR-negative).

Suppression of human HCC1954 breast cancer cell growth by MEDICA

HCC1954 growth was inhibited by shc-Src, dasatinib, shSTAT3, and P6 (Supplementary Fig. S2), indicating that both, c-Src and STAT3 drive oncogenesis in this cell line. Also,

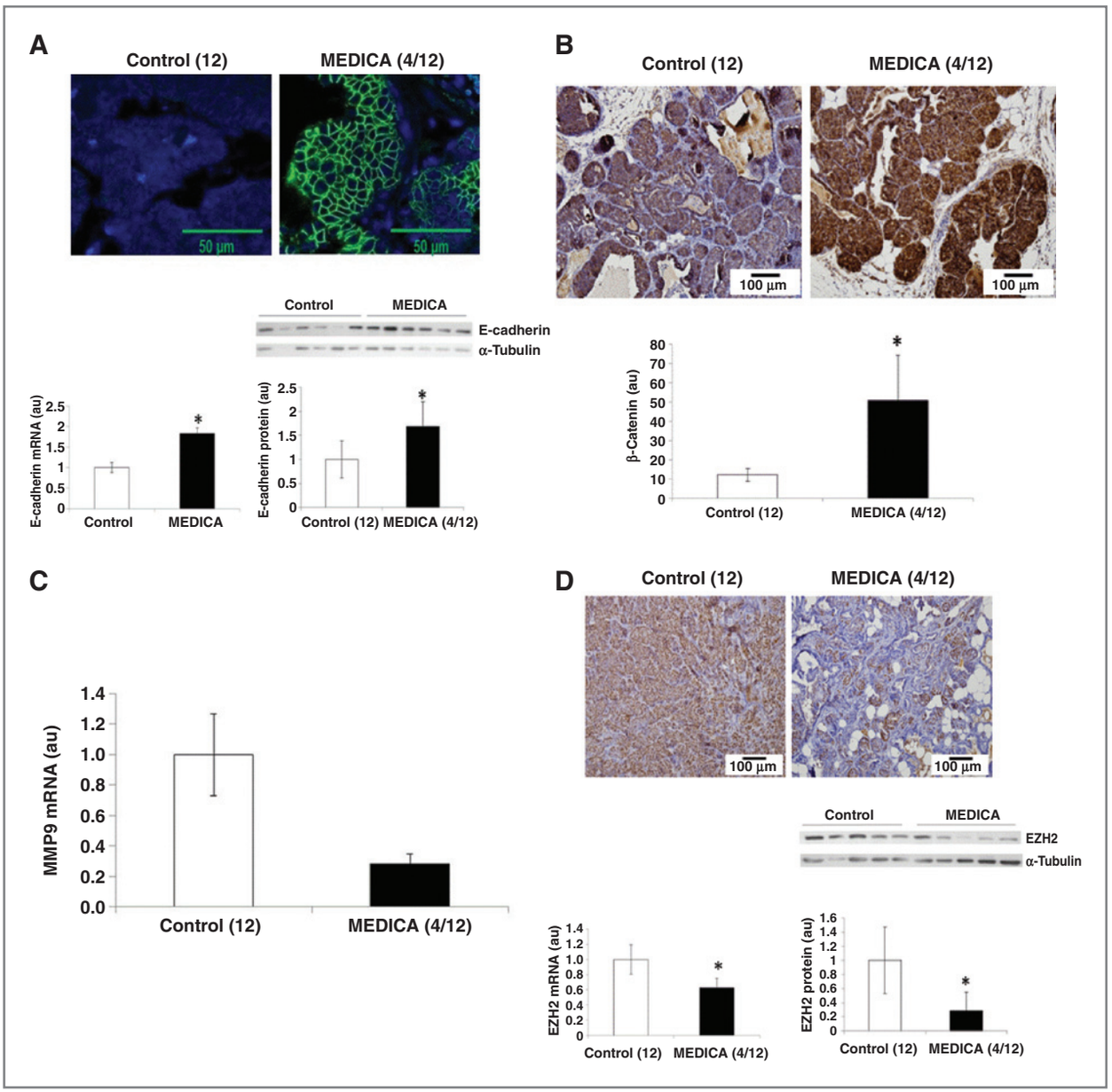

Figure 4. MMTV-PyMT MET in response to MEDICA. MMTV-PyMT female mice were fed *ad libitum* with standard rodent diet (Telkad 2018) in the absence or presence of added MEDICA (0.04% w/w) from weeks 4 to 12 (4/12). Representative immunostained photomicrographs of E-cadherin (A), β-catenin (B), and EZH2 (D) of MMTV-PyMT tumors of control and MEDICA (4/12)-treated mice. Total membranous β-catenin–stained area was determined by screening the β-catenin–stained area of 10 field per mouse using computerized microscopy. E-Cadherin (A), EZH2 (D), and MMP9 (C) transcripts were determined in respective tumor samples by qRT-PCR as described in Materials and Methods using HPRT1 as reference. E-Cadherin (A) and EZH2 (D) protein content normalized by tubulin was determined in respective tumor lysates by Western blotting as described in Materials and Methods. Mean ± SE (n = 6-8); *, significant as compared with control ($P < 0.05$).

dasatinib failed to suppress STAT3(Tyr705) phosphorylation, whereas P6 failed to suppress c-Src(Tyr416) phosphorylation (not shown), indicating that, similarly to PyMT cells, HCC1954 cell survival was independently driven by the two concerned oncogenes.

MEDICA treatment suppressed HCC1954 cell growth and clonogenity (Fig. 6A). Similarly to MEDICA effects in primary PyMT and in Met-1 cells (Fig. 5B), growth inhibition of HCC1954 cells was accompanied by abrogating the STAT3 and Akt transduction pathways (Fig. 6B). Also, MEDICA efficacy in suppressing growth of HCC1954 cells was partly abrogated in cells infected with shc-Src (Fig. 6B), implying c-Src as MEDICA target in suppressing HCC1954 growth.

Similarly to abrogating the c-Src/PyMT association in Met-1 cells (Fig. 5C), MEDICA treatment of HCC1954 cells resulted in increase in c-Src oligomers and other nonidentified high-

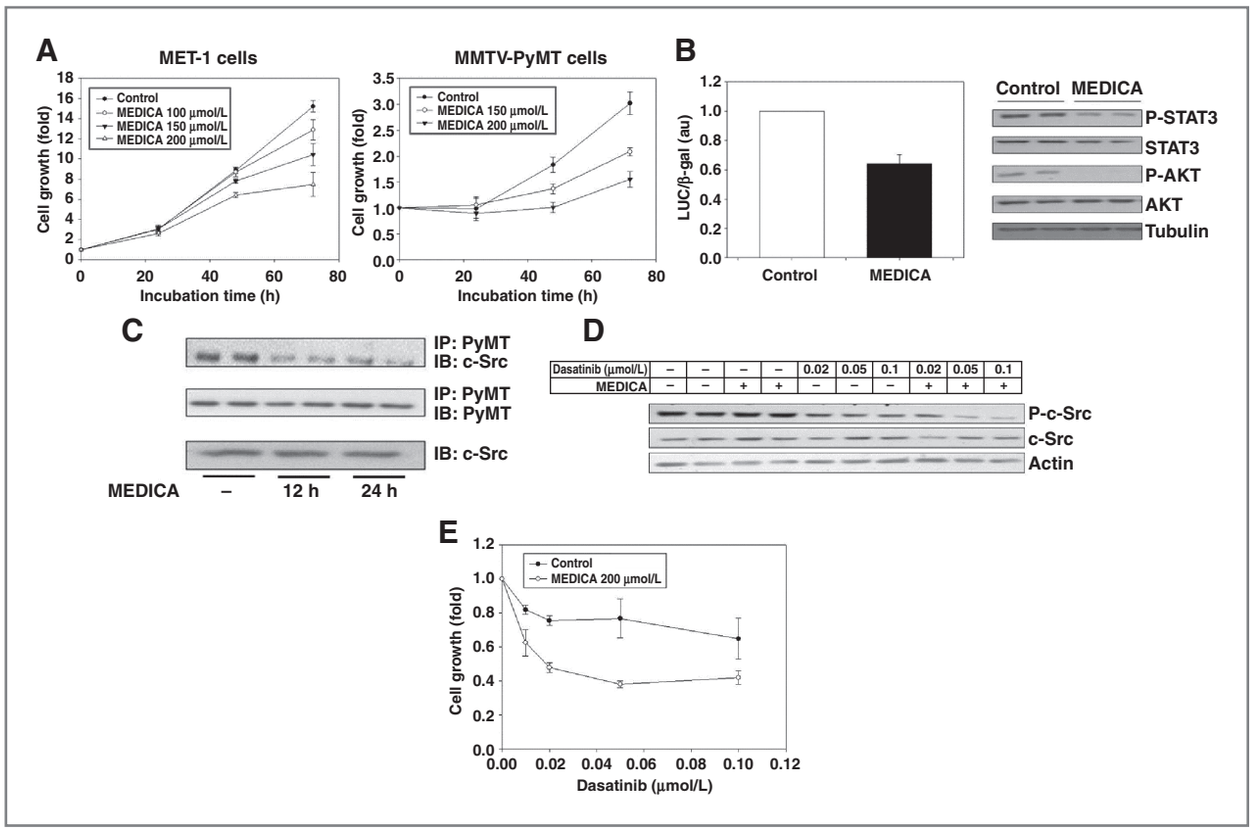

Figure 5. Suppression of MMTV-PyMT c-Src and STAT3 transduction by MEDICA. A, primary MMTV-PyMT cells and Met-1 cells were cultured in the presence of MEDICA as indicated. Cell growth was measured by the methylene blue method. Cell density on day 0 is defined as 1.0. Representative experiment. B, left, Met-1 cells were transfected with STAT3 reporter plasmid and constitutive STAT3 expression plasmid, followed by incubating the cells for 24 hours in the absence or presence of 200 μmol/L MEDICA as described in Materials and Methods. Luciferase activity of control cells is defined as 1.0 mean ± SE of three independent experiments; *, significant as compared with control ($P < 0.05$). Right, primary MMTV-PyMT cells were cultured for 24 hours in the absence or presence of 200 μmol/L MEDICA. Tumor lysates were subjected to SDS-PAGE as described in Materials and Methods. Representative experiment of three different preparations of primary MMTV-PyMT cells. C, Met-1 cells were cultured in the absence or presence of 200 μmol/L MEDICA for 12 and 24 hours as indicated. Cell lysates were immunoprecipitated by anti-PyMT antibody, followed by immunoblotting with anti-PyMT or anti–c-Src antibody as indicated. Bottom, c-Src input. Representative experiment. D, Met-1 cells were treated with 200 μmol/L MEDICA for 24 hours, followed by added dasatinib as indicated for the last 2 hours. Cell lysates were subjected to SDS-PAGE and analyzed by immunoblot for phospho–c-Src(Tyr416) as described in Materials and Methods. Representative experiment. E, Met-1 cells were grown for 24 hours with increasing concentrations of dasatinib as indicated in the presence or absence of 200 μmol/L MEDICA added 1 hour before dasatinib. Cell growth was measured by the methylene blue method. Cell density without additions is defined as 1.0. Representative experiment.

molecular weight adducts, with concomitant decrease in the c-Src monomers, exemplified by SDS-PAGE under nonreducing conditions (Fig. 6C). In line with that, and in apparent similarity to classical c-Src kinase inhibitors, MEDICA-induced c-Src oligomerization resulted in suppressing the phosphorylation of downstream substrates of c-Src, like FAK(Tyr925) or p130CAS(Tyr410) (Fig. 6D). Surprisingly, however, decrease in c-Src monomers and its activity by MEDICA treatment was accompanied by MEDICA-induced increase in Tyr416 phosphorylation of c-Src monomers and oligomers (Figs. 6E), implying that c-Src conformational change induced by MEDICA may account for its inactivation, while paradoxically increasing its Tyr416 phosphorylation.

Cysteine oxidation of c-Src by ROS (e.g., O_2^-, H_2O_2) has recently been reported to result in c-Src homodimerization (35) and in autophosphorylating its Tyr416 (36, 37), while activating (36) or inhibiting (35, 38) its kinase activity. Indeed, MEDICA treatment of HCC1954 cells resulted in increase in ROS production and H_2O_2 release into the culture medium, with concomitant decrease in the GSH/GSSG ratio (Fig. 6F). ROS production by MEDICA was similarly observed in Met-1 cells, being abrogated by added N-acetyl cysteine (NAC; not shown). MEDICA-induced c-Src oligomerization and c-Src (Tyr416) autophosphorylation were all abrogated by added NAC (Fig. 6G), implying that c-Src oxidation by MEDICA-induced ROS may account for suppressing its activity in the breast cancer context. Also, suppression of HCC1954 clonogenity by MEDICA was partly abrogated by added PEG–SOD (Fig. 6H), implying that MEDICA-induced ROS may partly account for growth inhibition of breast cancer cells. Moreover, ketogenic diets were reported to sensitize lung cancer cells to radiation-induced cell killing by a mechanism that appeared to

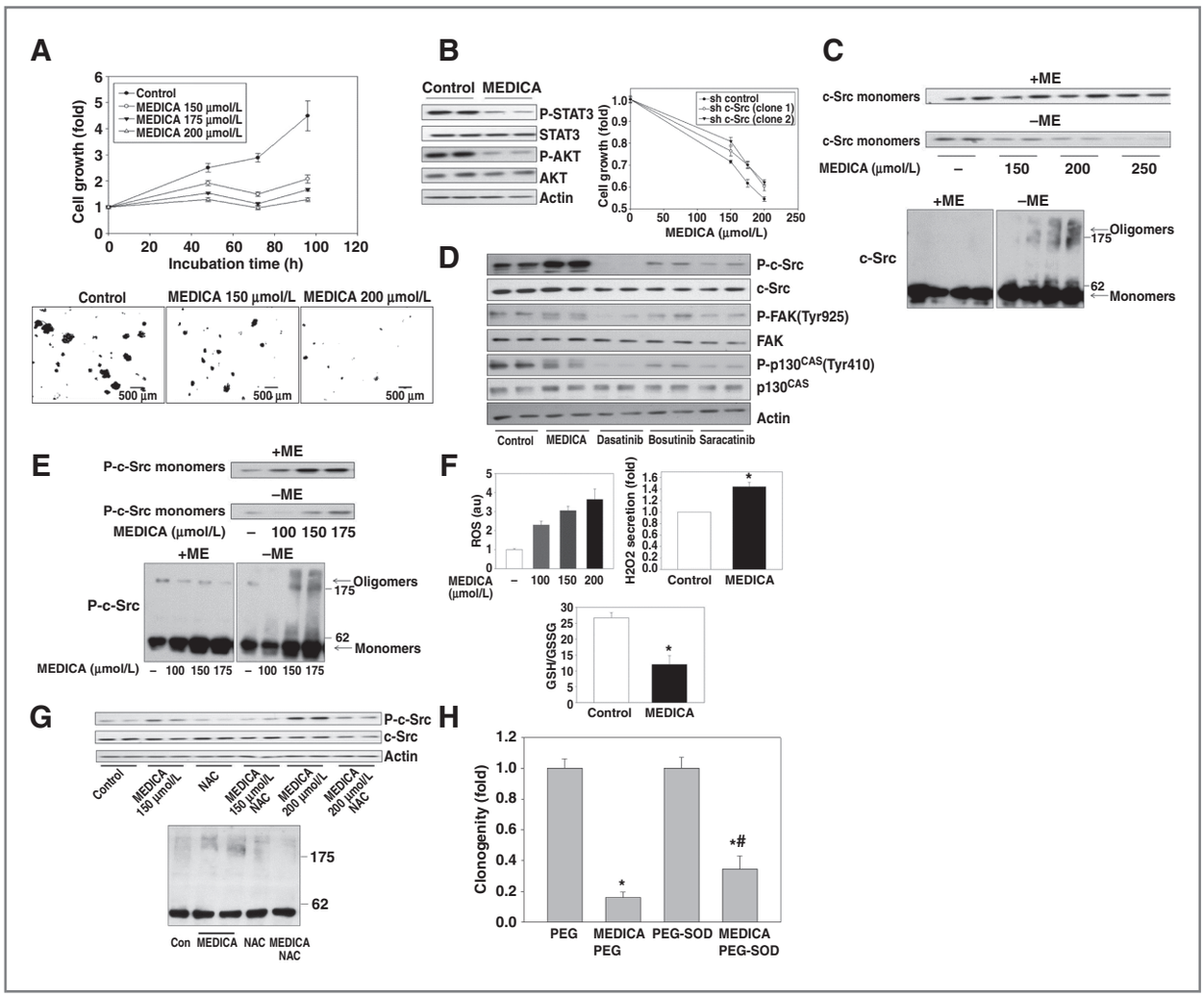

Figure 6. Suppression of HCC1954 tumorigenesis by MEDICA. A, top, HCC1954 cells were cultured in the presence of MEDICA as indicated. Cell growth was measured by the methylene blue method. Cell density without addition is defined as 1.0. Representative experiment. Bottom, HCC1954 cells were cultured for 24 hours in the presence of MEDICA as indicated. Cells were trypsinized and subjected to clonogenic assay. Colonies exceeding 400 μm in size were counted. Representative images. B, left, HCC1954 cells were cultured for 24 hours in the presence of 200 μmol/L MEDICA. Cell lysates were subjected to SDS-PAGE as described in Materials and Methods. Representative experiment. Right, HCC1954 cells were infected with sh-c-Src or sh-scramble as indicated, followed by culturing the cells for 48 hours with MEDICA as indicated. Cell growth was measured by the methylene blue method. Respective cell densities in the absence of added MEDICA are defined as 1.0. Representative experiment. C, HCC1954 cells were treated for 24 hours with MEDICA as indicated. Cell lysates were prepared in SDS sample buffer with or without mercaptoethanol, subjected to SDS-PAGE, and analyzed by immunoblot for c-Src monomers and oligomers. D, HCC1954 cells were treated for 24 hours with 200 μmol/L MEDICA, or for 2 hours with 0.2 μmol/L dasatinib, 1.0 μmol/L bosutinib (SKI606), or 1.0 μmol/L saracatinib as indicated. Cell lysates were subjected to SDS-PAGE as described in Materials and Methods. Representative experiment. E, HCC1954 cells were treated for 24 hours with MEDICA as indicated. Cell lysates were prepared in SDS sample buffer with or without mercaptoethanol, subjected to SDS-PAGE, and analyzed by immunoblot for phospho-c-Src(Tyr416). F, HCC1954 cells were treated for 4 to 5 hours in triplicates with MEDICA as indicated. ROS production was determined by DCF fluorescence, H_2O_2 release into the culture medium was determined by HRP/Amplex Red reagent, and the GSH/GSSG ratio was determined by the luminescence-based system as described in Materials and Methods. ROS production and H_2O_2 release of control cells are defined as 1.0 mean ± SE; *, significant as compared with the respective control ($P < 0.05$). G, top, HCC1954 cells were treated for 24 hours with MEDICA as indicated and 10 mmol/L NAC added 1 hour before MEDICA. Cell lysates were subjected to SDS-PAGE as described in Materials and Methods. Representative experiment. Bottom, HCC1954 cells were treated for 24 hours with 150 μmol/L MEDICA and 10 mmol/L NAC added 1 hour before MEDICA. Cell lysates were subjected to SDS-PAGE without mercaptoethanol as described in Materials and Methods, and analyzed by immunoblot for c-Src. Representative experiment. H, HCC1954 cells were cultured for 24 hours in the presence of 200 μmol/L MEDICA, 8 μgr/mL PEG or 100 U/mL PEG–SOD (Sigma) as indicated. Cells were trypsinized and subjected to clonogenic assay as described in Materials and Methods. Colonies exceeding 400 μm in size were counted. Clonogenity in the presence of PEG or PEG–SOD alone is defined as 1.0 mean ± SE of three independent experiments; *, significant as compared with the respective control ($P < 0.05$); #, significant as compared with MEDICA/PEG ($P < 0.05$).

involve oxidative stress (39). In mimicking that efficacy of ketogenic diets, pretreatment of HCC1954 cells with MEDICA, followed by their irradiation, resulted in amplified suppression of their clonogenity (Supplementary Fig. S3), implying the prospective efficacy of MEDICA in sensitizing tumor cells to radiation treatment.

Discussion

Seventy percent of human breast cancers express active c-Src, whereas 50% express constitutive STAT3 (12, 13). Furthermore, c-Src is reported to be a common oncogenic driver of variable trastuzumab resistance pathways, implying that suppressing its activity may overcome resistance (40). Similarly, STAT3 plays an essential role in breast cancer stem cells, being correlated with tamoxifen resistance (41). Hence, treatment strategies for suppressing the c-Src/STAT3 interplay are of relevance in treating human breast cancer (14).

c-Src plays an obligatory role in inducing breast cancer in MMTV-PyMT transgenic mice, in which membranous PyMT phosphorylation by c-Src results in cell proliferation and survival (42). Hence, the c-Src/PyMT complex may be visualized as oncogenic human RTK, with c-Src acting as its obligatory tyrosine kinase. Concomitantly, PyMT cell survival is promoted by constitutive STAT3 (5). Similarly to the MMTV-PyMT model, survival of human HCC1954 breast cancer cells is shown here to be driven by both, c-Src and STAT3. Of note, the c-Src and STAT3 oncogenic drivers are shown here to act independently in promoting MMTV-PyMT as well as HCC1954 cell survival, underscoring the need for abrogating both to suppress breast cancer.

Suppression of MMTV-PyMT and HCC1954 cell survival by MEDICA is shown here to be partly accounted for by suppressing the STAT3 transduction pathway, in line with our previous reports in other cell types (26). Suppression of STAT3 in MMTV-PyMT and HCC1954 cells by MEDICA is reflected by decrease in phospho-STAT3(Tyr705) and in STAT3 transcriptional activity. Suppression of cell survival by MEDICA is further due to MEDICA-induced ROS production, resulting in inactive c-Src that fails to activate its downstream substrates (35, 38). Thus, MEDICA treatment is shown here to abrogate c-Src association with its PyMT scaffold, as well as to suppress the phosphorylation of c-Src downstream substrates like FAK (Ser925) and p130CAS(Tyr410) in HCC1954 cells. That is despite enhancing c-Src(Tyr416) autophosphorylation, implying a mode of inhibition of c-Src–transforming activity that differs from that of classical c-Src kinase inhibitors (e.g., dasatinib, saracatinib, bosutinib; ref. 43).

c-Src oxidation has been reported to result in its heterodimerization and inactivation (35), whereas others have reported increase in c-Src Tyr416 phosphorylation, resulting in enhancing its kinase activity, tumorigenesis, and metastasis (36, 37, 44). Increase in c-Src(Tyr416) autophosphorylation and enhanced kinase activity has been ascribed to c-Src oxidation that results in a covalent S–S bond between its SH2 Cys245 and Cys487 of its kinase domain (37). In contrast, oxidation of Cys277 in c-Src GQGCFG glycine loop is reported to result in c-Src oligomerization and loss of c-Src activity (35), due presumably to decrease in c-Src affinity for its downstream substrates. Of note, oxidation of c-Src by MEDICA-induced ROS is shown here to result in abrogating c-Src kinase and transforming activity, while concomitantly increasing its Tyr416 phosphorylation, implying that the two oxidative modes of modulating c-Src activity are not mutually exclusive. Indeed, concomitant c-Src oxidation by the two oxidative modes may result in inactive c-Src oligomers having an "open" conformation with increase in c-Src(Tyr416) autophosphorylation (Figs. 6D and G).

Suppression of MMTV-PyMT tumor by MEDICA resulted in suppressing tumor mass, proliferation, mitotic index, and angiogenesis, while promoting tumor apoptosis. Most importantly, suppression of tumor survival was accompanied by increase in breast markers of differentiation, as evident by tumors consisting of papillary glandular structures, with cysts lined by squamous epithelium filled with fluid containing casein. Similar differentiation profile has previously been reported in MMTV-PyMT transgenic mice treated with the c-Src kinase inhibitor bosutinib (SKI606; ref. 45) as well as in c-Src–null mice (42), implying that inhibiting c-Src activity by kinase inhibitors, genetically, or by its oxidation may converge onto a similar phenotype.

Suppression of MMTV-PyMT tumor growth by MEDICA is further shown here to be accompanied by suppressing lung metastasis. Suppression of lung metastasis may be ascribed to suppressing the primary tumor, resulting in decreased probability for tumor dissemination, complemented by inhibiting epithelial–mesenchymal transition (EMT) of tumor cells. Indeed, MEDICA treatment was found to induce the enrichment of tumor cells with membranous E-cadherin and β-catenin, accompanied by decrease in MMP9 transcript. Because both, STAT3 and c-Src are potent inducers of EMT (46, 47), tumor cell epithelialization by MEDICA may partly be ascribed to abrogating EMT. EMT suppression by MEDICA may further be partly accounted for by suppressing Ezh2 transcription. Because Ezh2 is involved in controlling cell proliferation, differentiation, and apoptosis (31, 32), its suppression by MEDICA may further account for suppressing tumor growth while promoting tumor differentiation.

Suppression of MMTV-PyMT tumor growth by MEDICA apparently simulates that of ketogenic diet, indicating that the efficacy of carbohydrate-restricted/ketogenic diets in suppressing tumorigenesis may perhaps reflect the inherent tumor-suppressive efficacy of free LCFA or their respective CoA-thioesters, if allowed to reach high enough intracellular concentrations, by suppressing their esterification into lipids due to limiting insulin and glycerol-3-phosphate. The apparent similar phenotypes induced by MEDICA treatment and ketogenic diets may indicate that both may converge to the same target(s). Indeed, the induced increase in total body energy turnover by the two concerned effectors may perhaps point to mitochondria being the target of both effectors. Indeed, LCFA as well as MEDICA compounds have been previously reported to induce low-conductance gating of the mitochondrial permeability transition pore (PTP; refs. 48, 49). PTP gating results in robust increase in oxygen consumption due to decrease in inner mitochondrial membrane potential, and in increase in mitochondrial ROS production due to loss of mitochondrial reductive components (50). Because the compliance to ketogenic diets is quite poor, MEDICA treatment may offer the benefit of simulating carbohydrate restriction while maintaining a balanced diet.

Disclosure of Potential Conflicts of Interest

Jacob Bar-Tana has ownership interest (including patents) in SyndromeX. No potential conflicts of interest were disclosed by the other authors.

Authors' Contributions

Conception and design: U. Gluschnaider, R. Hertz, J. Bar-Tana
Development of methodology: U. Gluschnaider, R. Hertz, E. Pikarsky
Acquisition of data (provided animals, acquired and managed patients, provided facilities, etc.): U. Gluschnaider, R. Hertz, S. Ohayon, E. Smeir, M. Smets
Analysis and interpretation of data (e.g., statistical analysis, biostatistics, computational analysis): U. Gluschnaider, R. Hertz, S. Ohayon, E. Pikarsky, J. Bar-Tana
Writing, review, and/or revision of the manuscript: U. Gluschnaider, R. Hertz, E. Pikarsky, J. Bar-Tana
Administrative, technical, or material support (i.e., reporting or organizing data, constructing databases): U. Gluschnaider
Study supervision: U. Gluschnaider, J. Bar-Tana
Other (review of the article): U. Gluschnaider, E. Pikarsky

Acknowledgments

The authors thank Dr. Itay Ben-Porat for introducing us to the MMTV-PyMT model and Inbal Shamir for assistance in immunohistochemistry.

The costs of publication of this article were defrayed in part by the payment of page charges. This article must therefore be hereby marked *advertisement* in accordance with 18 U.S.C. Section 1734 solely to indicate this fact.

Received February 8, 2014; revised September 17, 2014; accepted September 17, 2014; published OnlineFirst October 10, 2014.

References

1. Fluck MM, Schaffhausen BS. Lessons in signaling and tumorigenesis from polyomavirus middle T antigen. Microbiol Mol Biol Rev 2009;73:542–63.
2. Lin EY, Jones JG, Li P, Zhu L, Whitney KD, Muller WJ, et al. Progression to malignancy in the polyoma middle T oncoprotein mouse breast cancer model provides a reliable model for human diseases. Am J Pathol 2003;163:2113–26.
3. Zhou AY, Ichaso N, Adamarek A, Zila V, Forstova J, Dibb NJ, et al. Polyomavirus middle T-antigen is a transmembrane protein that binds signaling proteins in discrete subcellular membrane sites. J Virol 2011;85:3046–54.
4. Carmichael GG, Schaffhausen BS, Dorsky DI, Oliver DB, Benjamin TL. Carboxy terminus of polyoma middle-sized tumor antigen is required for attachment to membranes, associated protein kinase activities, and cell transformation. Proc Natl Acad Sci U S A 1982;79:3579–83.
5. Garcia R, Yu CL, Hudnall A, Catlett R, Nelson KL, Smithgall T, et al. Constitutive activation of Stat3 in fibroblasts transformed by diverse oncoproteins and in breast carcinoma cells. Cell Growth Differ 1997;8:1267–76.
6. Bromberg JF, Horvath CM, Besser D, Lathem WW, Darnell JEJr. Stat3 activation is required for cellular transformation by v-src. Mol Cell Biol 1998;18:2553–8.
7. Silva CM. Role of STATs as downstream signal transducers in Src family kinase-mediated tumorigenesis. Oncogene 2004;23:8017–23.
8. Sansone P, Bromberg J. Targeting the interleukin-6/Jak/stat pathway in human malignancies. J Clin Oncol 2012;30:1005–14.
9. Yang Y, Jiang B, Huo Y, Primo L, Dahl JS, Benjamin TL, et al. Shp2 suppresses PyMT-induced transformation in mouse fibroblasts by inhibiting Stat3 activity. Virology 2011;409:204–10.
10. Arulanandam R, Geletu M, Raptis L. The simian virus 40 large tumor antigen activates cSrc and requires cSrc for full neoplastic transformation. Anticancer Res 2010;30:47–53.
11. Vultur A, Arulanandam R, Turkson J, Niu G, Jove R, Raptis L. Stat3 is required for full neoplastic transformation by the Simian Virus 40 large tumor antigen. Mol Biol Cell 2005;16:3832–46.
12. Ottenhoff-Kalff AE, Rijksen G, van Beurden EA, Hennipman A, Michels AA, Staal GE. Characterization of protein tyrosine kinases from human breast cancer: involvement of the c-src oncogene product. Cancer Res 1992;52:4773–8.
13. Chang Q, Bournazou E, Sansone P, Berishaj M, Gao SP, Daly L, et al. The IL-6/JAK/Stat3 feed-forward loop drives tumorigenesis and metastasis. Neoplasia 2013;15:848–62.
14. Bjorge JD, Pang AS, Funnell M, Chen KY, Diaz R, Magliocco AM, et al. Simultaneous siRNA targeting of Src and downstream signaling molecules inhibit tumor formation and metastasis of a human model breast cancer cell line. PLoS ONE 2011;6:e19309.
15. Klement RJ, Kammerer U. Is there a role for carbohydrate restriction in the treatment and prevention of cancer? Nutr Metab 2011;8:75.
16. Fine EJ, Segal-Isaacson CJ, Feinman RD, Herszkopf S, Romano MC, Tomuta N, et al. Targeting insulin inhibition as a metabolic therapy in advanced cancer: a pilot safety and feasibility dietary trial in 10 patients. Nutrition 2012;28:1028–35.
17. Tognon CE, Sorensen PH. Targeting the insulin-like growth factor 1 receptor (IGF1R) signaling pathway for cancer therapy. Expert Opin Ther Targets 2012;16:33–48.
18. Koppenol WH, Bounds PL, Dang CV. Otto Warburg's contributions to current concepts of cancer metabolism. Nat Rev Cancer 2011;11:325–37.
19. Ferguson RD, Gallagher EJ, Scheinman EJ, Damouni R, LeRoith D. The epidemiology and molecular mechanisms linking obesity, diabetes, and cancer. Vitam Horm 2013;93:51–98.
20. Gonzalez-Baro MR, Lewin TM, Coleman RA. Regulation of Triglyceride Metabolism. II. Function of mitochondrial GPAT1 in the regulation of triacylglycerol biosynthesis and insulin action. Am J Physiol Gastrointest Liver Physiol 2007;292:G1195–9.
21. Bar-Tana J, Ben-Shoshan S, Blum J, Migron Y, Hertz R, Pill J, et al. Synthesis and hypolipidemic and antidiabetogenic activities of beta,beta',beta'-tetrasubstituted, long-chain dioic acids. J Med Chem 1989;32:2072–84.
22. Bar-Tana J, Rose-Kahn G, Frenkel B, Shafer Z, Fainaru M. Hypolipidemic effect of beta, beta'-methyl-substituted hexadecanedioic acid (MEDICA 16) in normal and nephrotic rats. J Lipid Res 1988;29:431–41.
23. Mayorek N, Kalderon B, Itach E, Bar-Tana J. Sensitization to insulin induced by beta,beta'-methyl-substituted hexadecanedioic acid (MEDICA 16) in obese Zucker rats *in vivo*. Diabetes 1997;46:1958–64.
24. Russell JC, Amy RM, Graham SE, Dolphin PJ, Wood GO, Bar-Tana J. Inhibition of atherosclerosis and myocardial lesions in the JCR:LA-cp rat by beta, beta'-tetramethylhexadecanedioic acid (MEDICA 16). Arterioscler Thromb Vasc Biol 1995;15:918–23.
25. Qian B, Deng Y, Im JH, Muschel RJ, Zou Y, Li J, et al. A distinct macrophage population mediates metastatic breast cancer cell extravasation, establishment and growth. PLoS ONE 2009;4:e6562.
26. Zatara G, Hertz R, Shaked M, Mayorek N, Morad E, Grad E, et al. Suppression of FoxO1 activity by long-chain fatty acyl analogs. Diabetes 2011;60:1872–81.
27. Livak KJ, Schmittgen TD. Analysis of relative gene expression data using real-time quantitative PCR and the 2(-Delta Delta C(T)) Method. Methods 2001;25:402–8.
28. Kleer CG, Cao Q, Varambally S, Shen R, Ota I, Tomlins SA, et al. EZH2 is a marker of aggressive breast cancer and promotes neoplastic transformation of breast epithelial cells. Proc Natl Acad Sci U S A 2003;100:11606–11.
29. Shi B, Liang J, Yang X, Wang Y, Zhao Y, Wu H, et al. Integration of estrogen and Wnt signaling circuits by the polycomb group protein EZH2 in breast cancer cells. Mol Cell Biol 2007;27:5105–19.
30. Li X, Gonzalez ME, Toy K, Filzen T, Merajver SD, Kleer CG. Targeted overexpression of EZH2 in the mammary gland disrupts ductal

morphogenesis and causes epithelial hyperplasia. Am J Pathol 2009; 175:1246–54.
31. Chase A, Cross NC. Aberrations of EZH2 in cancer. Clin Cancer Res 2011;17:2613–8.
32. Zeidler M, Kleer CG. The Polycomb group protein enhancer of Zeste 2: its links to DNA repair and breast cancer. J Mol Histol 2006;37:219–23.
33. Borowsky AD, Namba R, Young LJ, Hunter KW, Hodgson JG, Tepper CG, et al. Syngeneic mouse mammary carcinoma cell lines: two closely related cell lines with divergent metastatic behavior. Clin Exp Metastasis 2005;22:47–59.
34. Montero JC, Seoane S, Ocana A, Pandiella A. Inhibition of SRC family kinases and receptor tyrosine kinases by dasatinib: possible combinations in solid tumors. Clin Cancer Res 2011;17:5546–52.
35. Kemble DJ, Sun G. Direct and specific inactivation of protein tyrosine kinases in the Src and FGFR families by reversible cysteine oxidation. Proc Natl Acad Sci U S A 2009;106:5070–5.
36. Giannoni E, Buricchi F, Raugei G, Ramponi G, Chiarugi P. Intracellular reactive oxygen species activate Src tyrosine kinase during cell adhesion and anchorage-dependent cell growth. Mol Cell Biol 2005;25: 6391–403.
37. Giannoni E, Taddei ML, Chiarugi P. Src redox regulation: again in the front line. Free Radic Biol Med 2010;49:516–27.
38. Tang H, Hao Q, Rutherford SA, Low B, Zhao ZJ. Inactivation of SRC family tyrosine kinases by reactive oxygen species *in vivo*. J Biol Chem 2005;280:23918–25.
39. Allen BG, Bhatia SK, Buatti JM, Brandt KE, Lindholm KE, Button AM, et al. Ketogenic diets enhance oxidative stress and radio-chemotherapy responses in lung cancer xenografts. Clin Cancer Res 2013;19:3905–13.
40. Zhang S, Huang WC, Li P, Guo H, Poh SB, Brady SW, et al. Combating trastuzumab resistance by targeting SRC, a common node downstream of multiple resistance pathways. Nat Med 2011;17:461–9.
41. Wang X, Wang G, Zhao Y, Liu X, Ding Q, Shi J, et al. STAT3 mediates resistance of CD44(+)CD24(-/low) breast cancer stem cells to tamoxifen *in vitro*. J Biomed Res 2012;26:325–35.
42. Guy CT, Muthuswamy SK, Cardiff RD, Soriano P, Muller WJ. Activation of the c-Src tyrosine kinase is required for the induction of mammary tumors in transgenic mice. Genes Dev 1994;8:23–32.
43. Creedon H, Brunton VG. Src kinase inhibitors: promising cancer therapeutics? Crit Rev Oncog 2012;17:145–59.
44. Kopetz S, Lesslie DP, Dallas NA, Park SI, Johnson M, Parikh NU, et al. Synergistic activity of the SRC family kinase inhibitor dasatinib and oxaliplatin in colon carcinoma cells is mediated by oxidative stress. Cancer Res 2009;69:3842–9.
45. Hebbard L, Cecena G, Golas J, Sawada J, Ellies LG, Charbono A, et al. Control of mammary tumor differentiation by SKI-606 (bosutinib). Oncogene 2011;30:301–12.
46. Canel M, Serrels A, Miller D, Timpson P, Serrels B, Frame MC, et al. Quantitative *in vivo* imaging of the effects of inhibiting integrin signaling via Src and FAK on cancer cell movement: effects on E-cadherin dynamics. Cancer Res 2010;70:9413–22.
47. Masuda M, Wakasaki T, Suzui M, Toh S, Joe AK, Weinstein IB. Stat3 orchestrates tumor development and progression: the Achilles' heel of head and neck cancers? Curr Cancer Drug Targets 2010;10: 117–26.
48. Samovski D, Kalderon B, Yehuda-Shnaidman E, Bar-Tana J. Gating of the mitochondrial permeability transition pore by long chain fatty acyl analogs *in vivo*. J Biol Chem 2010;285:6879–90.
49. Schonfeld P, Wojtczak L. Fatty acids as modulators of the cellular production of reactive oxygen species. Free Radic Biol Med 2008; 45:231–41.
50. Zorov DB, Juhaszova M, Sollott SJ. Mitochondrial ROS-induced ROS release: an update and review. Biochim Biophys Acta 2006; 1757:509–17.